

Seismic Response of Slab-Column Connection with Pyramid Shaped Drop Panel



Ahmed I., Hilal A., Mohamed Husain

Abstract: Both experimental and finite element analysis (FEA) was used to study the seismic response of reinforced concrete (RC) interior slab-column connection made with pyramid-shaped drop panel subjected to vertical and horizontal loads. The dimensions of the models at $1/4$ " linear scale for laboratory testing and FE Analysis (FEA) are derived from rules for dimensions of column drops, given a prototype "9.60m" grid and a slab thickness of "320mm". Lab specimens were tested with the drops (flat slab, rectangular and pyramid-shaped) facing up, with loadings (vertical down and horizontal in grid direction) applied by jacks towards the top of a central projecting "150mm" square column. One flat slab ("80mm" thick no drop), tested to failure under vertical load (80kN), provided values for setting variables used in the FEA. The remaining 5 lab specimens (1 flat and 1 each rectangular and pyramid-shaped 40mm and 30mm drop thicknesses), under a fixed vertical load (40kN), were tested to failure by increasing a moment at the column slab junction applied by a horizontal load to the column "500mm" above the slab. FEA results for the same conditions compared closely with experimental results. The pyramid-shaped drop models, with equal thickness to the rectangular drop models at the column faces (drops of "40mm" and "30mm"), exhibit similar maximum force resistances to the rectangular drop models. However, these resistances were achieved in the pyramid drops at higher maximum deflections – deflections being measured downwards at column centerline one half of slab thickness away from the face. A parametric study was conducted by FEA, at constant load, in vertical steps (10kN; 25kN 55kN), calculating deflections under increasing horizontal load. Calculations were made on the following definitions: Energy absorption is represented by the area under the deflection vs horizontal load curves; Ductility is the ratio of deflection at maximum to deflection at yield, and Stiffness and Overstrength factors are the slopes of the deflection load diagrams in the elastic and plastic zones respectively. Both drop type models exhibit significantly improved performance compared to the models without drops. The pyramid-shaped drop models exhibited improved energy absorption, ductility, and stiffness and overstrength compared to the rectangular drop models of the same column face thickness.

Keywords: Punching Shear Capacity; Slab Column Connection; Drop Panel; Pyramid-Shaped Drop Panel.

Manuscript received on 02 April 2021.

Revised Manuscript received on 18 June 2022.

Manuscript published on 30 June 2022.

* Correspondence Author

Ahmed Ibrahim*, Bachelor of Civil Engineering, Faculty of Engineering, Misr Higher Institute of Engineering and Technology, Egypt. E-mail: ahmedfrotly16@gmail.com

Dr. Hilal Abd Elkader, Ass. Prof., Department of Structural Engineering, Faculty of Engineering, Zagazig University, Egypt. E-mail: hilalcivil@yahoo.com

Prof. Mohamed M. Husain, Department of Concrete Structures, Faculty of Engineering, Zagazig University, Egypt. E-mail: mo_husain2000@yahoo.com

© The Authors. Published by Blue Eyes Intelligence Engineering and Sciences Publication (BEIESP). This is an [open access](https://creativecommons.org/licenses/by-nc-nd/4.0/) article under the CC-BY-NC-ND license <http://creativecommons.org/licenses/by-nc-nd/4.0/>

Retrieval Number: 100.1/ijeat.D23970410421

DOI: 10.35940/ijeat.D2397.0611522

Journal Website: www.ijeat.org

I. INTRODUCTION

Flat-slab systems are worrying because of the possibility of punching shear (PS) failure, which is brittle and could lead to catastrophic structural collapse. Present design rules for PS failure are based mainly on studies of the behaviour and strength of simply supported, conventional specimens extending to the nominal line of contraflexure (Alam, 1997 [1]; Kuang and Morley, 1992 [6]). The code provisions rely mostly on empirical methods derived from the results of tests on simply supported conventional (Selim and Sebastian, 2003) [12][13] and thin-slab specimens (Lovrovich and McLean, 1990 [8]). The Eurocode does not cover flat-slab frames as part of the lateral load resisting system, instead requiring them to comply with classification as secondary elements. As such, they are required to remain elastic while continuing to support gravity loading when subjected to the displacements associated with the most unfavourable seismic design conditions. By contrast, ACI 318-14 (Building Code Requirements for Structural Concrete (with Commentary)) allows intermediate moment frames (two-way slabs without beams) to be used as seismic resisting elements in SD Category C areas (moderate seismic hazard areas, such as South Africa). Clauses dealing with flat-slab frames as part of the lateral load resisting system are included in the currently proposed revisions to Eurocode 8. In a continuous flat slab, no panel edge can rotate freely, and some codes allow it to resist seismic forces in less-active seismic areas with a specific degree of deformability to maintain drift compatibility of the flat slab and the lateral-load resisting system. Most international seismic design codes have recently been updated to include capacity design, which was first introduced in the New Zealand seismic code in the mid-1970s (Paulay and Priestley, 1992 [10]; Seismic Response Evaluation of Flat Slab Structures, 2008 [11]; Effects of Stud Rails on Resistance of Edge Slab-Column Connections, 2010, Tunc 28-30 [3]). Capacity design results in structures that are more ductile and that dissipate more seismically excited energy through the flexural yielding of specific locations of the structure while preventing the possibility of brittle failure. Well-designed shear reinforcement improves slab PS strength and ductility appreciably (Lips et al., 2012 [8]). Graf and Mehrain, 1992 [5] presented an evaluation of the seismic performance of a 14-storey non-ductile reinforced concrete (RC) building in California built in the mid-1960s. The building is referred to as being non-ductile because it was designed according to California code provisions before the 1976 seismic code. The building had spans of "7.60 m" in each direction, supported on square columns with a cross-sectional length of "760 mm".

Published By:
Blue Eyes Intelligence Engineering
and Sciences Publication (BEIESP)
© Copyright: All rights reserved.



Seismic Response of Slab-Column Connection with Pyramid Shaped Drop Panel

Each slab was "230 mm" thick with a pyramid-shaped drop panel around the column faces. The building had survived two major seismic events, namely the 1971 San Fernando Valley earthquake and the 1989 Loma Prieta earthquake. In the present research, the behaviour of an interior slab-column connection thickened using a pyramid-shaped drop panel is investigated. The study involves comparing the results obtained from experimental tests and finite-element analysis (FEA) of rectangular and pyramid-shaped drop panels as slab-column interior connections and evaluating the energy absorption capacity, the ductility factor, stiffness and overstrength factor. Overall, the specimens with a pyramid-shaped drop panel performed better than did those with a rectangular drop panel.

II. EXPERIMENTAL PROGRAM

2.1. Model Geometry

The dimensions of the test specimens were a quarter of those of the interior slab-column connection for a prototype structure with equal spans of "9.60 m" as shown in Figure (1).

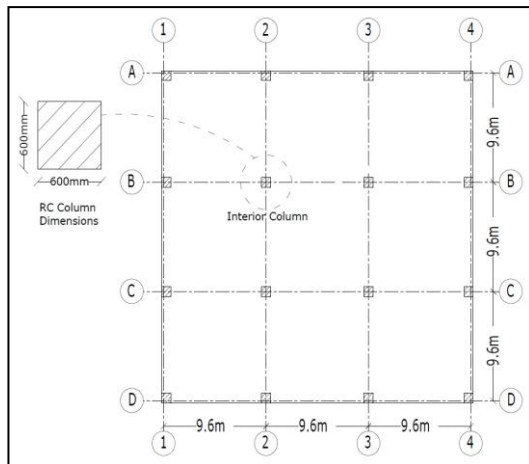


Fig. (1) Interior slab column connection in flat slab

The dimensions and thickness of the drop panel were chosen according to (ECP 203, 2018 [2]) equations (1) and (2)

$$\frac{Span}{3} \leq X \leq \frac{Span}{2}$$

$$\frac{t_s}{4} \leq t_d \leq \frac{t_s}{2}$$

Where "X" and "t_d" are the cross-sectional length and the thickness, respectively, of the drop panel and "t_s" is the thickness of the slab. Table (1) summarize various specimens' geometry.

Table (1) Specimens' geometry

Specimen	Slab Dimension (mm)	Drop Dimension (mm)	Drop Shape	Column Dimension (mm)
S01	1200X1200X80 Thickness	-	No Drop	150x150 x500 Height
S02		-	No Drop	
S2		800x800x40 Thickness	Rectangular	
S3		800x800x40 Thickness	Pyramid	
S4		800x800x30 Thickness	Rectangular	
S5	800x800x30 Thickness	Pyramid		

2.2. Material Properties

2.2.1. Concrete Mixture

The properties of the hardened concrete were tested at "7" and "28" days to achieve a compressive strength "f_{cu}" of 25 MPa after "28" days. Table (2) gives the average values of "f_{cu}" for eight standard cubes with a cubic length of "150 mm" according to (ECP 203, 2018 [2]), these having been made during the concrete pouring process.

Table (2) Compressive strength after "7" and "28" days

Pouring Days	(f _{cu}) after 7 Days (Mpa)	(f _{cu}) after 28 Days (Mpa)
Day 1	21	26
Day 2	20	24
Day 3	22	26

2.2.2 Reinforcing Bars

The compression reinforcement in a slab was 10Ø6 (yield strength f_y = "240 MPa"; ultimate strength f_u = "350 MPa") in each direction. The tensile reinforcement was 10Ø8 (f_y = "240 MPa"; f_u = "350 MPa") in each direction. The column reinforcement was 4Ø12 (f_y = "360 MPa"; f_u = "520 MPa") and the stirrups were 7Ø8 (f_y = "240 MPa"; f_u = "350 MPa"). The rectangular drop-panel reinforcement was 6Ø6 (f_y = "240 MPa"; f_u = "350 MPa") in each direction, and the pyramid-shaped drop-panel reinforcement was 12Ø6 (f_y = "240 MPa"; f_u = "350 MPa"). Figures (2-4) show all six specimens.

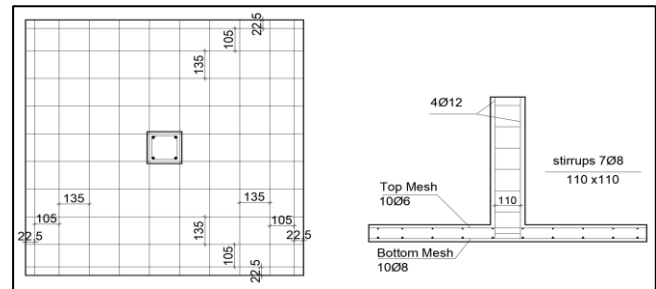


Fig. (2) Specimens (S01) & (S02) with no drops

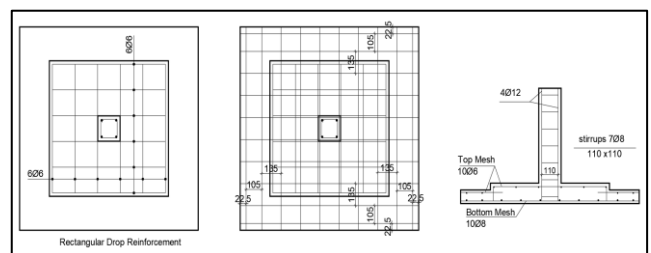


Fig. (3) Specimen (S2) & (S4) with rectangular drop

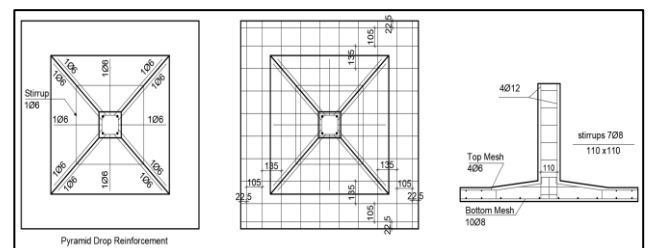


Fig. (4) Specimen (S3) & (S5) with pyramid drop

2.3. Loading Procedure

In the absence of a shaking table and because of laboratory limitations, loads were applied statically using hydraulic jacks on top of the column. The loading procedure had two stages, namely (i) applying a constant vertical load and then (ii) applying a horizontal load until failure. The magnitude of the ultimate PS force P_u was calculated according to (ECP 203, 2018 [2]), using equations (3), (4) and (5) as following:

$$b_0 = 2 \times (b_1 + b_2) = 840\text{mm} \quad (3)$$

$$q_{cup,uncracked} (N/mm^2) = 0.316 \left(0.5 + \frac{a}{b} \right) \sqrt{\frac{f_{cu}}{\gamma_c}} = 1.94 N/mm^2 \quad (4)$$

$$= \text{the least of} \left[\begin{array}{l} 0.316 \left(0.5 + \frac{a}{b} \right) \sqrt{\frac{f_{cu}}{\gamma_c}} = 1.94 N/mm^2 \\ 0.8 \left(\frac{\alpha \times d}{b_0} + 0.2 \right) \sqrt{\frac{f_{cu}}{\gamma_c}} = 1.58 N/mm^2 \end{array} \right] \quad (5)$$

where " b_0 " is the control perimeter, " $q_{cup,uncracked}$ " is the allowable concrete stress, " a " and " b " are the column width and length, respectively, " d " is the slab effective depth, and the factor α equals 4, 3 or 2 for an interior, exterior or corner column, respectively. (ECP 203, 2018 [2]) states that $q_{up} \leq q_{cup,uncracked}$, therefore P_u can be calculated as

$$P_u = q_{cup,uncracked} \times d \times b_0 \cong 80 \text{ kN}.$$

From the calculations, the ultimate vertical load that causes PS is "80 kN". Specimen "S01" was tested to verify this value by applying a vertical load on the top of the column until failure; the experimental ultimate vertical load that caused PS failure was "80 kN", the same value as that from the calculations. For specimens "S02" to "S5", the first stage of loading (i.e. applying a constant vertical load) used "40 kN", which is "50%" of P_u to allow for a safety factor; for the second stage of loading, the horizontal load was applied gradually until the RC specimen failed.

III. EXPERIMENTAL SETUP

The available laboratory potential was not as required by the present study, this being because the available hydraulic jack was supported vertically on a steel frame with four steel columns. A steel base made of "HEB20" as shown in Figure (5) was used to lift the specimen to the correct level of an existing vertical hydraulic jack. The RC specimen was bolted to the steel base using eight high-strength bolts (HSB) M16 (Gr. 8.8) to obtain boundary condition at zero moments location, which is free to rotate with no translation, as shown in Figure (6). A new steel beam (also "HEB20") was connected to the existing columns by friction as shown in Figure (7), this being to support another cantilever steel beam (also "HEB20") with a hydraulic jack to apply a horizontal load on the top of the column after applying the desired vertical load by the existing hydraulic jack.



Fig. (5) Steel Base

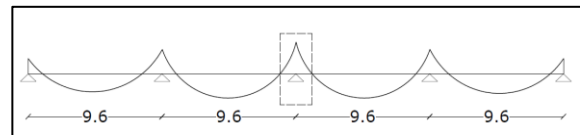


Fig. (6) The boundary condition at zero moments location



Fig. (7) Steel beam connected to the existing column

3.1 Measurements

Various continuous measurements were made during the tests. Load cells measured the applied loads at the hydraulic jacks, and a linear variable differential transducer (LVDT) was placed on the top side of the slab at a distance " $d/2$ " from the column face to measure the vertical deflection. Figure (8) shows the RC specimen ready to be tested.

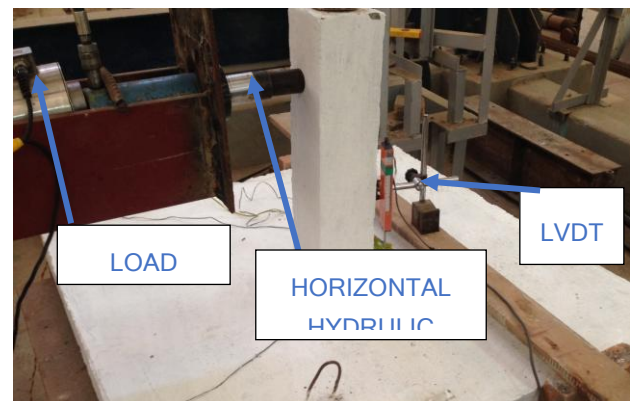


Fig. (8) Specimen ready for the test

IV. NUMERICAL ANALYSIS

4.1 Reinforced Concrete Modelling

The Abaqus software was used in (FEA). The CDP (concrete damaged plasticity) model offered in the Abaqus software was used to model the reinforced concrete, considering both tensile cracking and compressive crushing as possible failure modes (Lee and Fenves, 1998 [7]). In the CDP model, the behaviour of the concrete depends mainly on four constitutive parameters, namely (i) the dilation angle " ψ " measured in the "p-q" plane at high confining pressure, (ii) the flow potential eccentricity " e " of the potential plastic surface, (iii) the ratio of the initial biaxial compressive yield stress " f_{b0} " to the initial uniaxial compressive yield stress " f_{c0} " and (iv) the ratio " K_c " of the second stress invariant on the tensile meridian to that on the compressive meridian. Note that the former two parameters are used to describe the shape of the potential flow function according to a non-associative flow rule, while the latter two parameters are associated with the shape of the yield function. In the present work, the dilation angle was adjusted by trial and error within the range of "30–40°" to best correlate with the results of the experimental tests. The flow potential eccentricity " e " was taken as "0.1" as suggested by the Abaqus Analysis user manual. The value of " f_{b0}/f_{c0} " was obtained directly from a Kupfer curve. The default value for " K_c " was taken as "2/3", which is used commonly in practice and is also suggested in the Abaqus Analysis user manual. In addition to the aforementioned four parameters, the concrete's uniaxial compressive strength and Young's modulus were provided. Table (3) summarizes the material properties of the concrete used in the CDP model.

Table (2) Material properties for concrete in the CDP model

Material's Parameters		Plasticity parameters	
Concrete Compressive Strength (MPa)	25	ψ	30.0° ~ 40.0°
		e	0.1
Young's Modulus (MPa)	22000	f_{b0}/f_{c0}	1.16
Poisson's ratio	0.18	K_c	0.667
		Viscosity parameter	0.005

The rebar density was " $7.75 \times 10^{-5} \text{ N/mm}^3$ ", and the associated Young's modulus and Poisson ratio were "210 GPa" and "0.3", respectively. The value of f_y was "240 MPa" for the top/bottom mesh, drop reinforcing and stirrups were "360 MPa" for the column rebars. The concrete was modelled with three-dimensional (3D) eight-node hexahedral elements with reduced integration (C3D8R), and the flexural reinforcement was modelled with 3D two-node linear truss elements (T3D2). Perfect bonding was considered between the concrete and the reinforcement bars through the embedded method in the Abaqus software. The mesh size was "20 mm" based on previous research (Genikomsou and Polak, 2015 [4]).

4.2 Boundary Conditions

Quasi-static analysis in Abaqus/Explicit was considered in this study. Eight hinged supports were applied along the bottom edges of the specimen at the same positions as those

of the bolts. Translation was prohibited in all three directions ($R_x = R_y = R_z = 0$), whereas rotation was not ($U_x = U_y = U_z \neq 0$).

4.3 Loading Procedure

For verification purposes, the loading procedure used in the experimental tests was replicated in the FEA. The first stage involved applying a vertical pressure at the top of the column equivalent to the force measured experimentally divided by the area of the column ("150 mm" \times "150 mm"). The second stage involved applying horizontal pressure gradually at the top of the column until failure, which was considered as being when the solution in Abaqus failed to converge. The horizontal pressure applied at the top of the column was equal to the horizontal force obtained experimentally divided by the loaded area of "150 mm" (column width) \times "120 mm" (diameter of hydraulic-jack cylinder).

V. VERIFICATION

The results are presented as load-deflection curves to include the relationships between deflection and both vertical and horizontal load. The ultimate failure loads of the tested specimens are given in Table (4).

Table (3) Total loads and maximum deflection for test specimens

Specimens	Applied Loads (KN)		Maximum Deflection (mm)
	Vertical Load	Horizontal Load	
S01	80	0	10
S02	40	23	10
S2	40	44	12
S3	40	44	15
S4	40	41	11
S5	40	41	14

Figures (9–13) show the verifications for different specimens.

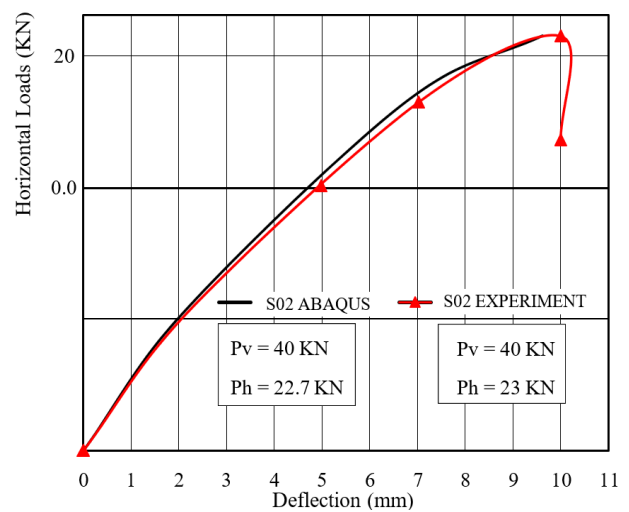


Fig. (9) Load-Deflection relationship for (S02) at "40KN" vertical load

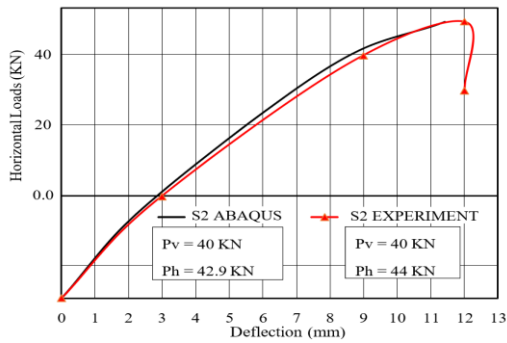


Fig. (10) Load-Deflection relationship for (S2) at "40kN" vertical load

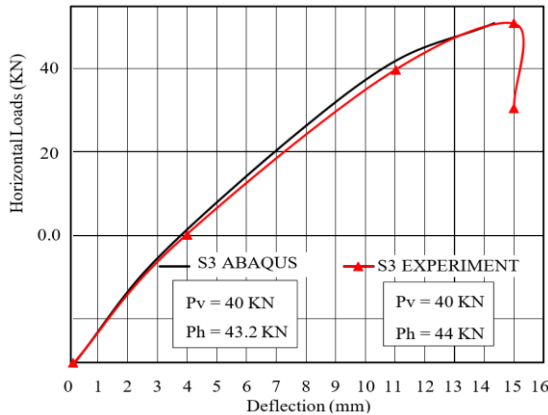


Fig. (11) Load-Deflection relationship for (S3) at "40kN" vertical load

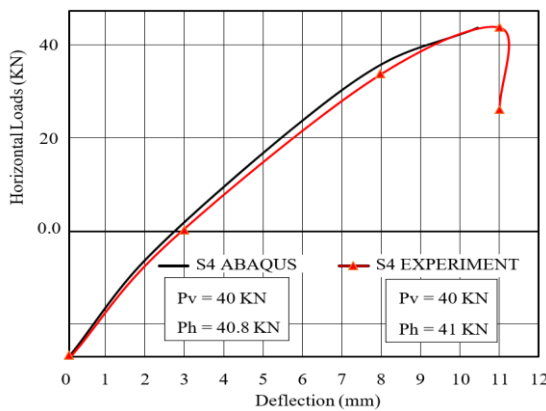


Fig. (12) Load-Deflection relationship for (S4) at "40kN" vertical load

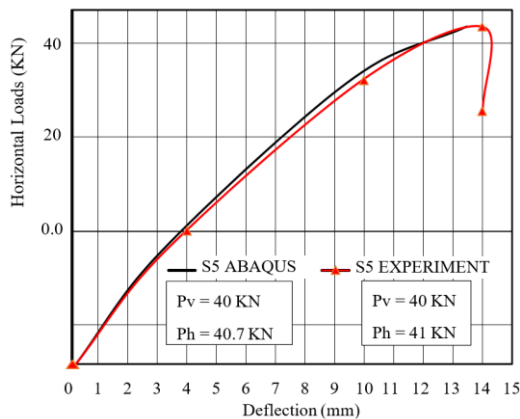


Fig. (13) Load-Deflection relationship for (S5) at "40kN" vertical load

Figure (14) shows the load-deflection comparison among specimens S02, S2 and S3, and Figure (15) does the same for specimens S02, S4 and S5.

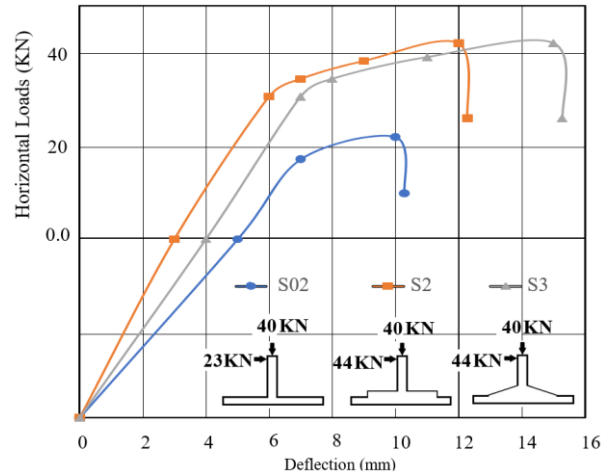


Fig. (14) Load-deflection relationship for specimens S02, S2 & S3 at "40kN" vertical load

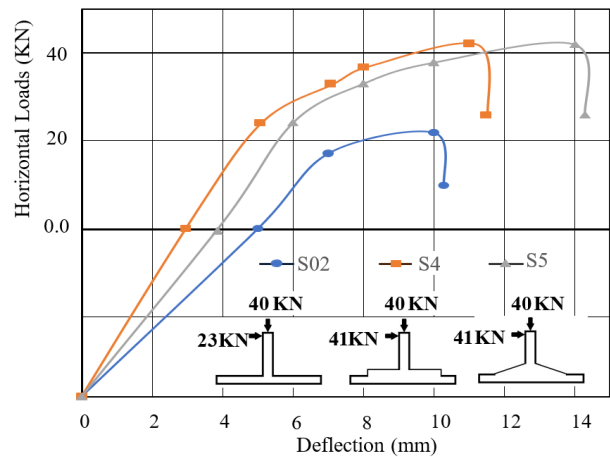


Fig. (15) Load-deflection relationship for specimens S02, S4 & S5 at "40kN" vertical load

In these comparisons, the results are close enough to justify using the same modelling technique for the subsequent parametric study.

VI. PARAMETRIC STUDY

FEA was used to study the behaviour of both rectangular and pyramid-shaped drop panels under the effect of vertical and horizontal forces at different values. The comparison is made between specimens S2 & S3 and S4 & S5. The experimental tests used a vertical load equal to 50% of P_u (40 kN), then the horizontal load was applied until failure. The values chosen for the vertical load in the parametric study were 12% of P_u (10 kN), 30% of P_u (25 kN) and 70% of P_u (55 kN).

6.1. Results Comparison Between (S2) & (S3)

Figures (16–18) show the load-deflection curves for specimens S02, S2 and S3 at a vertical load of "10 kN", "25 kN" and "55 kN", respectively.

Seismic Response of Slab-Column Connection with Pyramid Shaped Drop Panel

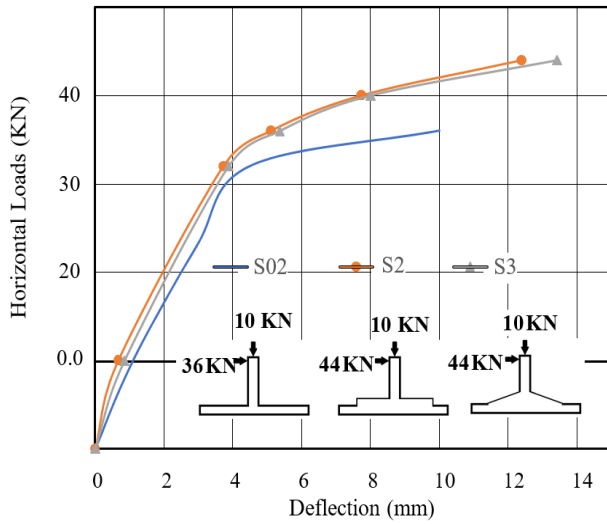


Fig. (16) Load-deflection curves for S02, S2 & S3 at VI. of "10kN"

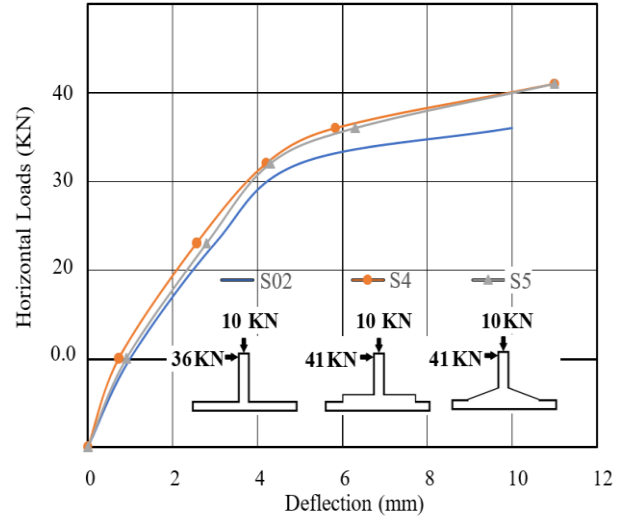


Fig. (19) Load-deflection curves for S02, S4 & S5 at VI. of "10kN"

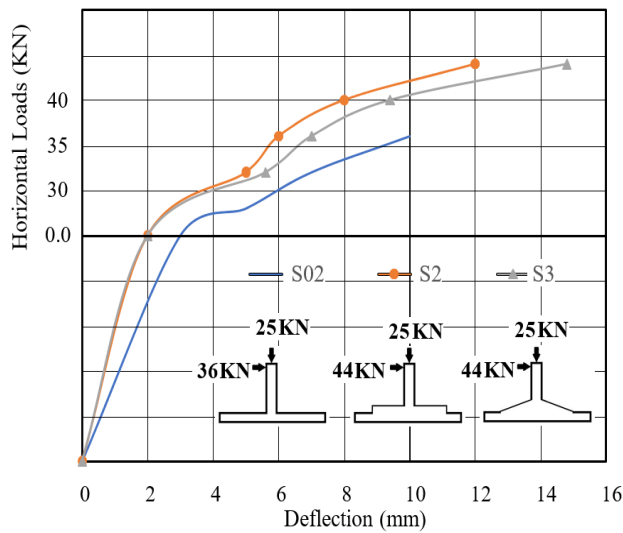


Fig. (17) Load-deflection curve for S02, S2 & S3 at VI. of "25kN"

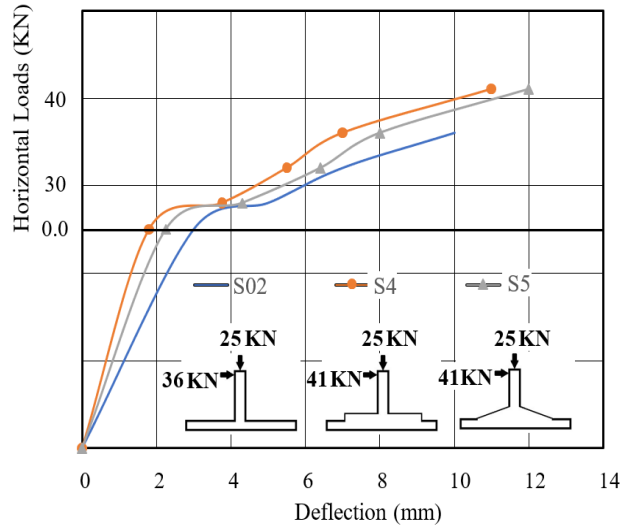


Fig. (20) Load-deflection curves for S02, S4 & S5 at VI. of "25kN"

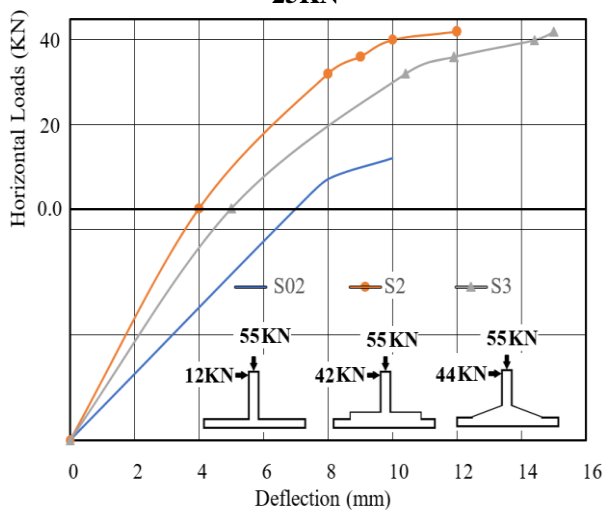


Fig. (18) Load-deflection curve for S02, S2 & S3 at VI. of "55kN"

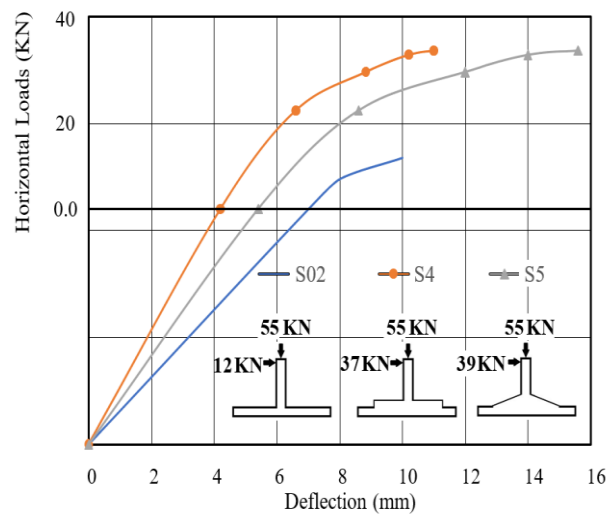


Fig. (21) Load-deflection curves for S02, S4 & S5 at VI. of "55kN"

6.2. Results Comparison Between (S4) & (S5)

Figures (19–21) show the load-deflection curves for specimens S02, S4 and S5 at a vertical load of "10 kN", "25 kN" and "55 kN", respectively.

6.3. Energy Absorption Capacity

The energy absorption capacity was calculated from the load-deflection curve. Table (5) shows different values of area under the load-deflection curve for every case.

Table (5) Energy absorption capacity for all specimens

Specimens	10KN vertical load applied
	The area under the load-deflection curve
S02	30.75
S2	46.1
S3	50.2
S4	34.8
S5	36.2
Specimens	25KN vertical load applied
	The area under the load-deflection curve
S02	38.32
S2	64.4
S3	76.3
S4	52.4
S5	56.8
Specimens	40KN vertical load applied
	The area under the load-deflection curve
S02	39.85
S2	74
S3	91.6
S4	61.4
S5	79
Specimens	55KN vertical load applied
	The area under the load-deflection curve
S02	40.7
S2	82.5
S3	98.5
S4	69.2
S5	97.4

6.4. Ductility

Two essential parameters for the code-based seismic design of structures are the strength modification factor and the displacement amplification factor. Strength modifications are commonly accounted using both a reduction factor due to nonlinear hysteretic behaviour and an amplification factor due to overstrength. The displacement ductility ratio is widely accepted as a useful performance indicator because of its apparent relationship with the strength reduction factor due to nonlinear hysteretic behaviour.

Ductility ratios are commonly expressed in terms of various response parameters related to deformations, namely displacements, rotations and curvatures. The displacement ductility ratio in cyclic loading is based on the envelope curve of the hysteretic loops that show the relation between the strength and displacement of a system or structural element. A typical envelope of the structural response is shown in Figure (22). Idealizing the actual structural response curve by the linearly elastic perfectly plastic curve, the displacement ductility ratio is defined as the ratio of maximum displacement (Δ_u) to the corresponding displacement at the onset of yielding (Δ_y) (Miranda and Bertero, 1994 [9]). The calculated value of (μ_Δ) for the test specimens are summarized in Table (6).

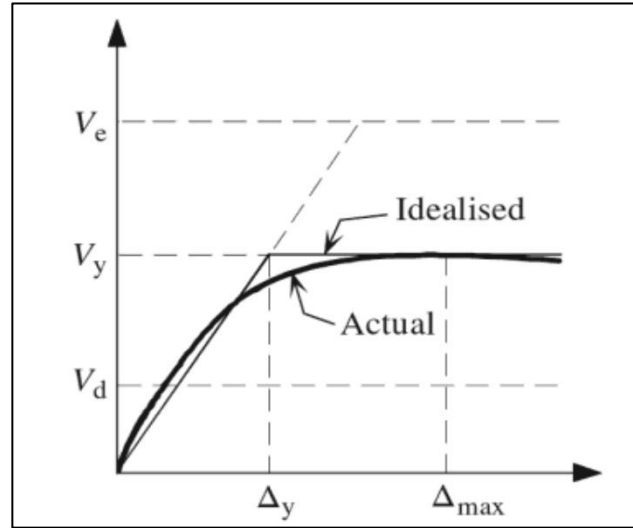


Fig. (22) The envelope of actual and idealized structural response

Table (6) Measured ductility for all specimens

Specimens	Vertical Load (KN)	Horizontal Load (KN)	Δ_y (mm)	Δ_u (mm)	μ_Δ
S02	25	36	6	10	1.67
S2	25	44	8	12	1.5
S3	25	44	7	14	2
S4	25	41	7	11	1.57
S5	25	41	5	12	2.4
S02	40	23	7	10	1.43
S2	40	44	8	12	1.5
S3	40	44	7	15	2.14
S4	40	41	7	11	1.57
S5	40	41	5	14	2.8
S02	55	12	7	10	1.43
S2	55	42	8	12	1.5
S3	55	44	6	15	2.5
S4	55	37	8	11	1.38
S5	55	39	6	15	2.5

6.5. Stiffness and Overstrength Factor

The stiffness " k_s " of an elastic body is a measure of its resistance to deflection or deformation. The stiffness of the RC slab-column connection was calibrated from the results of the tested specimens to capture the effect of vertical load on the connection stiffness. The overstrength factor " Q_o " indicates the resistance of the slab-column connection in the plastic zone. The stiffness and overstrength were obtained from the load-deflection curves of the test specimens. The stiffness of the slab-column connection was determined from the load-deflection curve by calculating the slope of the linear part in the elastic zone, while the overstrength is the slope of the curved line at the peak, as shown in Figure (23). The values of " k_s " and " Q_o " are given in Table (7).

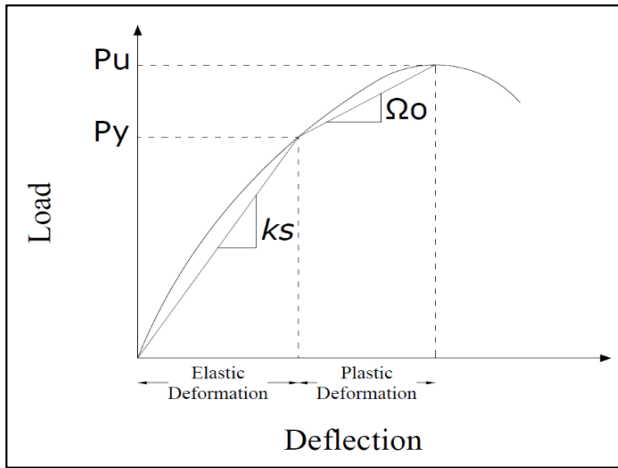


Fig. (23) Load deflection curve showing (k_s & Ω_o)

Table (7) Values of (k_s) and (Ω_o)

Specimens	Vertical Load (KN)	Horizontal Load (KN)	k_s	Ω_o
S02	25	36	8.6	1.1
S2	25	44	8.1	1
S3	25	44	8.7	1.17
S4	25	41	8.6	0.825
S5	25	41	10.2	1.83
S02	40	23	8.2	1.67
S2	40	44	9.7	1.5
S3	40	44	10.2	1.625
S4	40	41	10.1	2.25
S5	40	41	10.4	3.28
S02	55	12	7.8	4
S2	55	42	11	2.7
S3	55	44	11.3	4.23
S4	55	37	10.2	2.77
S5	55	39	10.8	3.82

VII. CONCLUSIONS

The following conclusions are drawn from the results presented herein. Increasing the thickness of the pyramid-shaped drop panel at the column face may increase the PS strength and thus also the resistance to lateral loads produced by earthquakes or wind loads before the joint collapses. The deflection values for the pyramid-shaped drop panel were larger than those for the rectangular drop panel.

This may be considered disadvantageous for pyramid-shaped drop panels regarding serviceability, but the pyramid-shaped drop panel had better ductility performance and energy absorption capacity. The FEA results showed that the reinforcement in the tension side of this connection had come close to the ultimate stress (360 MPa). The capacity of the connection to resist lateral loads is related to the vertical load, and it was found that when the vertical load was 70% of P_u , the connection failed when subjected to lower values of the horizontal load.

The inclination angle of the pyramid-shaped drop panel was between 5° and 7° , and increasing the inclination angle resulted in higher strength and ductility of the slab-column connection. The energy absorption capacities of the

pyramid-shaped and rectangular drop panels were 240% and 200% greater, respectively, than that of a specimen with no drop panel, showing that the pyramid-shaped drop panel offered an additional 40% improvement in capacity over the rectangular drop panel.

The vertical load affected the ductility factor of the interior slab-column connection. At a vertical load of 25 kN (i.e. 30% of P_u), the specimens with a rectangular drop panel behaved more rigidly than did the reference specimen or those with a pyramid-shaped drop panel. The specimens with a pyramid-shaped drop panel had 120% greater ductility at 30% of P_u . When the applied vertical load was greater than 50% of P_u , the specimens with a rectangular drop panel began to exhibit a degree of ductility and more PS strength compared to the reference specimen, but the specimens with a pyramid-shaped drop panel exhibited 180% greater ductility compared to those with a rectangular drop panel. The results for the overstrength factor indicated that the pyramid-shaped drop panel performed better in the plastic zone than did the rectangular drop panel, with an approximate increase of 70%.

DECLARATIONS

Availability of data and materials

The datasets used and/or analysed during the current study are available from the corresponding author on reasonable request.

Competing interests

The authors declare that they have no conflict of interest.

Funding Not applicable' for that section

AUTHORS' CONTRIBUTIONS

1.Ahmed Ibrahim, Bachelor of civil engineering: Researcher Student.

2.Hilal Abd Elkader, Ass. Prof. Dr. of Structural Engineering Department: Supervisor

3.Mohamed M. Husain, Prof. of Concrete Structures: Main Supervisor.

ACKNOWLEDGEMENTS

The author owes his thanks to the members of the technical staff of the civil engineering department at the faculty of engineering, Zagazig University, for their help in construction and testing the specimens.

REFERENCE

1. Alam, A.K.M. (1997). *Punching Shear Behaviour of Reinforcement Concrete Slabs*. M.Sc. Engineering Thesis.
2. ECP 203 (2018). *The Egyptian Code for Design and Construction of Concrete Structures*. Cairo: Egypt: Ministry of Housing.
3. Effects of Stud Rails on Resistance of Edge Slab-Column Connections. (2010). *American Society of Civil Engineer 6th International Engineering & Construction Conference*, pp.28–30. Cairo: Egypt.
4. Genikomsou, A.S. and Polak, M.A. (2015). *Damaged Plasticity Modelling of Concrete in Finite Element Analysis of Reinforced Concrete Slabs*. Waterloo, Canada. [CrossRef]
5. Graf, W.P. and Mehraim, M. (1992). *Analysis and testing of a flat slab concrete building*. Dames & Moore. Los Angeles, California: USA.



6. Kuang, J.S. and Morley, C.T. (1992). Punching Shear Behaviour of Restrained Reinforced Concrete Slabs. *ACI Structural Journal*, 89(1), pp.13–19. [[CrossRef](#)]
7. Lee, J. and Fenves, G.L. (1998). Plastic-damage model for cyclic loading of concrete structures. *Journal of Engineering Mechanics*, 124(8), pp.892–900. [[CrossRef](#)]
8. Lips, S. et al. (2012). Experimental Investigation on Punching Strength and Deformation Capacity of Shear-Reinforced Slabs. *ACI Structural Journal*, 109(6). [[CrossRef](#)]
9. Lovrovich, J.S. and McLean, D.I. (1990). Punching Shear Behaviour of Slabs with varying Span-Depth Ratios. *ACI Structural Journal*, 87(5), p.pp 507-511. [[CrossRef](#)]
10. Miranda, E. and Bertero, V.V. (1994). *Evaluation of strength reduction factors for earthquake-resistant design*. The Plymouth: United Kingdom. [[CrossRef](#)]
11. Paulay, T. and Priestley, M.J.N. (1992). *Seismic Design of Reinforced Concrete and Masonry Buildings*. [online] Wiley.com. Available at: <https://www.wiley.com/en-us>. [[CrossRef](#)]
12. Seismic Response Evaluation of Flat Slab Structures. (2008). *Proceedings of the Arab Colloquium on Disaster and Crisis Management*. Riyadh: Saudi Arabia.
13. Selim, W. and Sebastian, W.M. (2003). Punching Shear Failure in Reinforced Concrete Slabs with Compressive Membrane Action. *ACI Structural Journal*, 100(4), p.pp 471-479. [[CrossRef](#)]

AUTHOR PROFILE



Ahmed Mohsin Abdou Ibrahim, Researcher, and corresponding author. Graduated with a bachelor of civil engineering, Faculty of Engineering, Misr Higher Institute of Engineering and Technology 2012. Started academic path in 2015 for a master's degree in engineering science at Zagazig university. Funded the entire work including the experimental setup and test. E-mail: ahmedfroy16@gmail.com



Hilal Hassan Abd Elkader, Supervisor Prof. Dr. of Structural Engineering Department, Faculty of Engineering, Zagazig University. With 25 years of experience in teaching. Deeply invested in achieving tenure through administrative service committee contributions and an accomplishment-oriented approach to teaching. Dedicated to helping researchers to investigate deeply in themselves through their academic careers. E-mail: hilalcivil@yahoo.com



Mohamed Mahmoud Mohamed Husain, Main Supervisor Prof. Dr. of Concrete Structures, Faculty of Engineering, Zagazig University. Motivated and talented concrete structure professor driven to inspire students to pursue academic and personal excellence. Consistently strive to create challenging and engaging learning in which students become lifelong scholars and learners. E-mail: mo_husain2000@yahoo.com